Jacques Blanc-Talon · Rudi Penne
Wilfried Philips · Dan Popescu
Paul Scheunders (Eds.)

LNCS 10617

Advanced Concepts for Intelligent Vision Systems

18th International Conference, ACIVS 2017
Antwerp, Belgium, September 18–21, 2017
Proceedings

Springer

Lecture Notes in Computer Science 10617

Commenced Publication in 1973
Founding and Former Series Editors:
Gerhard Goos, Juris Hartmanis, and Jan van Leeuwen

More information about this series at http://www.springer.com/series/7412

Jacques Blanc-Talon · Rudi Penne
Wilfried Philips · Dan Popescu
Paul Scheunders (Eds.)

Advanced Concepts for Intelligent Vision Systems

18th International Conference, ACIVS 2017
Antwerp, Belgium, September 18–21, 2017
Proceedings

Springer

Editors
Jacques Blanc-Talon
DGA
Paris
France

Dan Popescu
CSIRO Data 61
Canberra, ACT
Australia

Rudi Penne
University of Antwerp
Antwerp
Belgium

Paul Scheunders
University of Antwerp
Wilrijk
Belgium

Wilfried Philips
Ghent University - imec
Ghent
Belgium

ISSN 0302-9743 ISSN 1611-3349 (electronic)
Lecture Notes in Computer Science
ISBN 978-3-319-70352-7 ISBN 978-3-319-70353-4 (eBook)
https://doi.org/10.1007/978-3-319-70353-4

Library of Congress Control Number: 2017959602

LNCS Sublibrary: SL6 – Image Processing, Computer Vision, Pattern Recognition, and Graphics

Printed on acid-free paper

This Springer imprint is published by Springer Nature
The registered company is Springer International Publishing AG
The registered company address is: Gewerbestrasse 11, 6330 Cham, Switzerland

Contents

Navigation, Mapping, Robotics and Transports

Video Processing and Retrieval

Security, Forensics, Surveillance

Image Processing

Omnidirectional Localization in vSLAM with Uncertainty Propagation and Bayesian Regression

David Valiente(✉), Óscar Reinoso, Arturo Gil, Luis Payá, and Mónica Ballesta

Systems Engineering and Automation Department,
Miguel Hernández University, Alicante, 03202 Elche, Spain
{dvaliente,o.reinoso,arturo.gil,lpaya,mballesta}@umh.es

Abstract. This article presents a visual localization technique based solely on the use of omnidirectional images, within the framework of mobile robotics. The proposal makes use of the epipolar constraint, adapted to the omnidirectional reference, in order to deal with matching point detection, which ultimately determines a motion transformation for localizing the robot. The principal contributions lay on the propagation of the current uncertainty to the matching. Besides, a Bayesian regression technique is also implemented, in order te reinforce the robustness. As a result, we provide a reliable adaptive matching, which proves its stability and consistency against non-linear and dynamic effects affecting the image frame, and consequently the final application. In particular, the search for matching points is highly reduced, thus aiding in the search and avoiding false correspondes. The final outcome is reflected by real data experiments, which confirm the benefit of these contributions, and also test the suitability of the localization when it is embedded on a vSLAM application.

Keywords: Omnidirectional images · Visual SLAM · Feature matching · Visual localization

1 Introduction

On mobile robotics, Simultaneous Localization and Mapping (SLAM) represents a crucial aspect. Such paradigm implies a simultaneous estimation of the map and the localization of the robot. This fact entails a real challenge when it comes to complexity, due to the incremental nature of the procedure, which is normally affected by non-linear inputs and noise, that gravely compromise the convergence of a sensitive system.

Under such circumstances, different research has been conducted. It is worth highlighting the evolution on the use of different kind of acquisition sensors. Initially, laser [14] and sonar [13] were widely acknowledged. However, more recently, there have been an incipient use of visual sensors like digital cameras,

J. Blanc-Talon et al. (Eds.): ACIVS 2017, LNCS 10617, pp. 263–274, 2017.
https://doi.org/10.1007/978-3-319-70353-4_23

which have emerged as one of the most reliable tools for gathering information of the environment. Comparing to former sensors, they become a promising alternative due to their low cost, lightness, low consumption, precision and efficiency to process visual data. Amongst others, omnidirectional cameras are remarkable for their capability to acquire large scenes on an only image, thanks to their large field of view. Different approaches have concentrated on computer vision techniques by using single cameras with visual encoding of 3D landmarks [11]; stereo-structure [6]; and omnidirectional cameras [4,16]. Specially, many contributions support matching systems relying on the image side [20], but also on the mapping side [2].

In this paper we also rely on the potentials of the matching in order to map visual information along different scenes during navigation tasks. Nonetheless, in contrast to general matching, we emphasize on the target application feedback. Dealing with a vSLAM approach implies that huge efforts have to be addressed to the management of the uncertainty and convergence [10,21]. That is the main reason why we intend to assess these variables, and use them as feedback to refine the standard matching, and thus the final estimation. Our approach seeks a more robust model which dynamically adapts to the current deviations in the system in terms of uncertainty. Therefore, we propose a robot localization model, which is solely based on omnidirectional images. In particular, we reinforce the matching process by means of the propagation of the current uncertainty of the system. We also introduce a Bayesian regression technique [17] so as to obtain a sensor data distribution [7], that allows to predict the probability of appearance of matching points. Synthesizing, the system operates as follows:

– Image acquisition at each SLAM iteration.
– Movement prediction (SLAM) and uncertainty propagation to the current image.
– Omnidirectional epipolarity determination on the second image frame.
– Global Bayesian inference for weighting and refining the final robust and reliable matching.

The remainder is: Sect. 2 presents the general characteristics of the omnidirectional system and the implemented epipolarity adaption to the omnidirectional geometry. Section 3 comprises the implementation of the omnidirectional visual localization. The propagation of uncertainty and regression inference are also highlighted within the contribution of the adaptive matching. Section 4 provides an overview to the view-based SLAM approach, with the omnidirectional localization embedded; Sect. 5 presents the real data results which assess the validity of the approach and the benefits of the research contributions; Sect. 6 exposes the main conclusions extracted from this work.

2 Omnidirectional Vision System

The vision system consists of a catadioptric set, conformed by an hyperbolic mirror jointly assembled with a CCD camera, as shown in Fig. 1, where the real

Fig. 1. Real equipment: (a) Pioneer P3-AT mounted with omnidirectional camera, internal odometer and laser range finder; (b) CCD FireWire DMK21BF04; (c) Eizho Wide 70 Mirror.

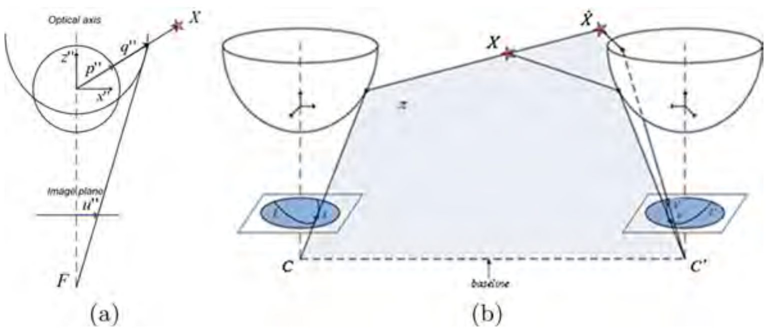

Fig. 2. (a) Mapping of a scene point to the image plane; (b) epipolar constraint adaptation to the omnidirectional geometry.

robotic system is also presented. The image generation is reproduced in Fig. 2. Note that the center of projection coincides with the focus of the hyperboloid. This coincidence represents the basis for the camera to focalize the 3D scene on the image frame.

Figure 2(a) shows how a scene point X directs $p'' = (x''^T, z'')$ in the same direction as q, which is projected to u'' on the image plane, being collinear to x''. Notice that the central sphere unifies the notation of the projection vectors for normalization purposes, as per calibration, regardless the characteristics of the mirror and its non-linearities. Thus the mapping of a 3D point onto the image plane is depicted, and analytically expressed as follows [9]:

$$\lambda p'' = \lambda \begin{bmatrix} u'' \\ a_0 + a_2||u''||^2 + \ldots + a_n||u''||^n \end{bmatrix} = PX \qquad (1)$$

where $P \in \mathbb{R}^{3x4}$ is the projection matrix, denoted as $P = [R|T]$, with R a rotation matrix $\in \mathbb{R}^{3x3}$ and T a translation $\in \mathbb{R}^3$ between camera and global reference system. The Taylor expansion refers to the particular projection model for each mirror, which is experimentally estimated by a calibration toolbox [18].

2.1 Epipolarity Definitions

The epipolar constraint [9] becomes a fundamental tool in order get motion recovery and therefore, for the computation of visual localization. The nature of our omnidirectional system forced us to redesign the planar epipolar constraint to the geometry of our camera system. This allows us to propose advanced techniques in terms of feature detection between two omnidirectional images, and likewise between two poses of the robot so as to localize it. To that purpose it is necessary to introduce the essential matrix, E_{3x3} [15], and its relation with two matched points between images, x and x'. By means of a given calibration, the corresponding points can be normalized to $\hat{x}$ and $\hat{x'}$:

$$\hat{x}'^T E \hat{x} = 0 \tag{2}$$

Finally, the elements in E entail a decomposition: R_{3x3} and $T = [t_x, t_y, t_z]$, as a general rotation and translation, through the skew symmetric $[T]_x$ [9]. In consequence, a 2D movement $\in$ XY, and angular movement (β, ϕ), between two poses of the robot, can be recovered up to scale factor, from:

$$E = [T]_x R = \begin{bmatrix} 0 & 0 & \sin(\phi) \\ 0 & 0 & -\cos(\phi) \\ \sin(\beta - \phi) & \cos(\beta - \phi) & 0 \end{bmatrix} \tag{3}$$

Such adaption to the omnidirectional geometry is expressed in Fig. 2(b). The projection of X on two image references, x and x', is determined by the epipolar plane, π, and both camera centers C and C'. An essential aspect is associated to l and l', as the epipolar lines which define the geometric place for matching points to lay on. This is crucial for us to design an advanced visual matching, which ultimately returns potential data for a robust localization.

Contrarily to traditional stereo-planar applications [3,19], here epipolar lines transform into ellipses as a result of the intersection of π with the hyperbolic mirror of the camera. In this sense, different contributions will be presented in the following sections, so as to come up with a robust visual localization, sustained by uncertainty propagation and bayesian techniques, with their basis relying on this epipolar adaption.

3 Omnidirectional Visual Localization

Our visual localization approach is sustained by the epipolar adaption presented above. As shown in (3), two poses of the robot can be solely related by matching points in two omnidirectional images acquired at such poses. That is, a motion transformation defined by an angular movement. Figure 3 synthesizes such image-to-pose equivalence in terms of movement. Therefore, a clear inference from (2) can be noted. Then, the localization between poses, Fig. 3(a), is transferred to a visual problem in Fig. 3(b).

On the analytical side, (2) can be posed as a linear system:

$$D_i e_i = \begin{bmatrix} x_0 z_1 & y_0 z_1 & z_0 x_1 & z_0 y_1 \end{bmatrix} \begin{bmatrix} e_1, e_2, e_3, e_4 \end{bmatrix}^T, \forall i \in [1, \dots, N] \tag{4}$$

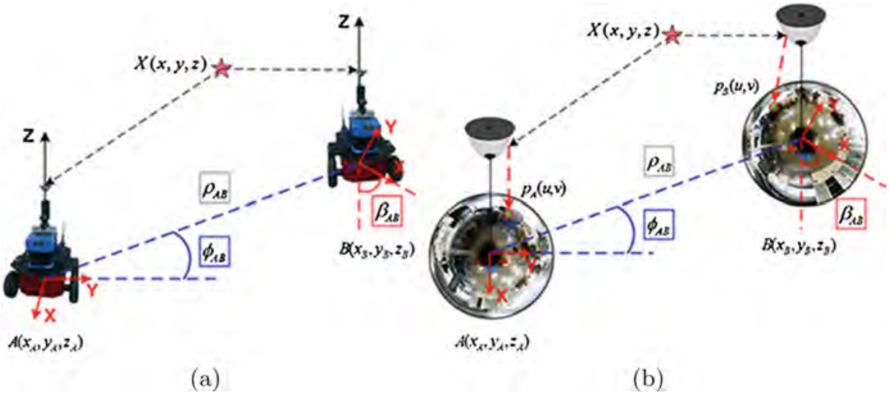

Fig. 3. Omnidirectional visual localization between poses A and B. (a) Robot reference system; (b) camera reference system. Projections, $p_A(u,v)$ and $p_B(u,v)$, are indicated.

where $\hat{x} = (x_0, y_0, z_0)$ and $\hat{x}' = (x_1, y_1, z_1)$ represent two matched points between image poses, and e_i the estimation terms in E, which encode the localization measures (β, ϕ). It is worth noting the low number of matching points needed, $N_{min} = 4$, for retrieving a motion estimation, since D_{Nx4}.

Finally [9] states the fundamentals for a Single Value Decomposition (SVD) of (3), which produces a quaternion set of solutions (β, ϕ), as two rotations and translations:

$$\phi = atan\frac{-e_1}{e_2}; \quad \beta = atan\frac{e_3}{e_4} + atan\frac{-e_1}{e_2} \tag{5}$$

$$t_{x1} = [\cos\phi, \sin\phi, 0]; \quad t_{x2} = t_{x1} + \pi; \quad R_1 = \begin{bmatrix} \cos\beta & -\sin\beta & 0 \\ \sin\beta & \cos\beta & 0 \\ 0 & 0 & 1 \end{bmatrix}; \quad R_2 = R_\pi R_1 \tag{6}$$

3.1 Uncertainty Propagation

Once the fundamentals for the omnidirectional localization have been described, now it necessary to detail the uncertainty propagation implementation. The aim is to enhance the matching by providing this process with the capability to adapt dynamically to the current noise of the system, and therefore to the associated uncertainty, at t. The final output, as a main contribution, is the reduction of the search area for matchings on the pixel side. To that end, the epipolar constraint, is again invoked (2). Particularly, current inconsistencies in the system, represented by uncertainty, are propagated through such constraint, which now accepts a dynamic threshold, $\delta(\hat{z}_t)$:

$$x'^T \hat{E} x < \delta(\hat{z}_t) \tag{7}$$

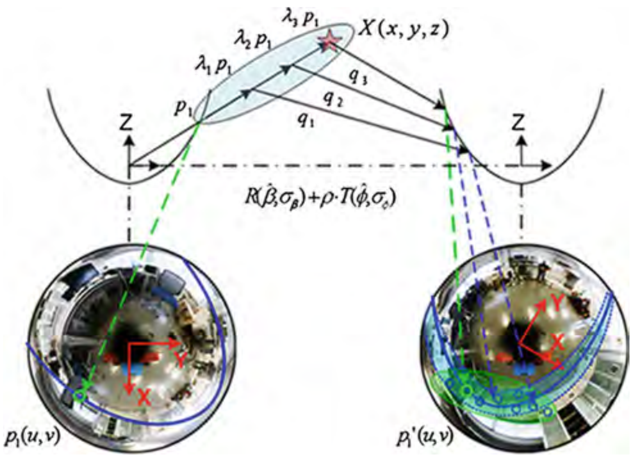

Fig. 4. Adaptive matching. p_1 establishes the multi-scaled distribution, $\lambda_i p_1$. q_i projects onto the second image by means of $R{\sim}\mathrm{N}(\hat{\beta}, \sigma_\beta)$, and $T{\sim}\mathrm{N}(\hat{\phi}, \sigma_\phi)$, (8). The result is a reduced search area (green). Epipolar curve transforms into an elliptic area (blue) due to the uncertainty propagation on (7). (Color figure online)

Note that this threshold depends on a predicted observation movement, $\hat{z}_t = (\hat{\beta}, \hat{\phi})$, as provided by a general vSLAM approach, which is implicitly related to the corresponding uncertainty of the system.

The innovation measured between consecutive states of the vSLAM system, S_t, represents a powerful tool to establish σ values for $\hat{z}_t$ by means of a predicted rotation, R, and translation, T:

$$S_t = \begin{bmatrix} \sigma_\phi^2 & \sigma_{\phi\beta} \\ \sigma_{\beta\phi} & \sigma_\beta^2 \end{bmatrix}; \quad R \sim N(\hat{\beta}, \sigma_\beta); \quad T \sim N(\hat{\phi}, \sigma_\phi) \tag{8}$$

This fact means that a predicted matching can be determined on the second image frame, even though when no feature detector has been used on the second frame. A gaussian multi-scale distribution, $\lambda_i p_1$, is generated on the first image frame, and then propagated on the second, q_i, by considering the uncertainty, (7), and the predicted movement (8). Figure 4 depicts the entire procedure for this adaptive matching, which eventually produces a reduced area where candidate matching points are found, rather than a global search over the entire image. The topology of the new search area corresponds to the reshaping of the epipolar constraint, which now transforms into a surface due to the effects of $\delta(\hat{z}_t)$. The ultimate stage involves a visual descriptor comparison, being $d_i(x)$ and $d'_j(x')$ the visual descriptors of two points in the first and second image respectively. Finally, a Mahalanobis metric (χ) is computed over them, so as to get an accepted visual distance in order to assume two feature points as a valid pair of matching points:

$$||d_i(x) - d'_j(x')|| \leq \chi[dim(z_t)] \tag{9}$$

3.2 Bayesian Regression

Having described the enhanced matching with uncertainty propagation, here we include a Bayesian regression technique such as Gaussian Processes (GP) [17] in order to obtain a sensor data distribution for the matching on the omnidirectional frame. GP is an advantageous regression technique since they do not need to extract conventional relations between inputs and outputs, contrarily to traditional inference. A GP produces a matching data distribution, which can be mapped onto a global reference system. This information is very useful in order to refine the search area for matching points. A GP, denoted as $f(x)$, is constituted by its mean, $m(x)$, covariance $k(x, x')$, and training and test input vectors, x and x' respectively.

$$f(x) \sim \mathcal{GP}[m(x), k(x, x')] \tag{10}$$

Assuming that the GP output provides the probability distribution of our matching, now we can fuse this probability with an information metric into the entire process, so as to reinforce the procedure and to reduce even more the matching detection area. This provides a reliable refinement feedback. In terms of the selected metric, we chose an information-based one [12], Kullback-Leibler divergence (KL):

$$KL(F_1 \parallel F_2) = \sum_{i=1}^{k} F_1(i) \log \frac{F_1(i)}{F_2(i)} \tag{11}$$

We pursue the assessment of the fluctuation in the position of the matching points on the global system. Under this situation, KL can measure such variations between matching points detected on a previous pair of images, F_1, and the new matching points on the next pair F_2. The value of KL encodes relevant variations on the position of the matching points along the navigation of the vehicle. The higher KL value, the newer visual information detected by the robot. Therefore, the candidate matchings, can also be weighted by such metric, which determines the probability areas were a corresponding point is more likely to be found. The graphical result for this probability distribution is presented in Fig. 5, where two consecutive pair of images are compared by being passed through the adaptive matching process, already described in the previous section, and now fused with the GP regression.

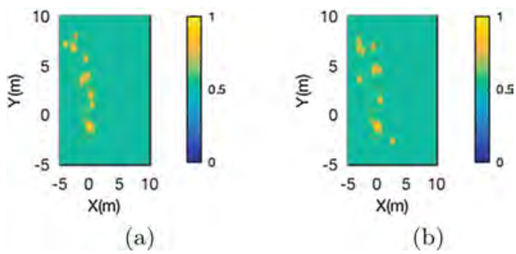

Fig. 5. Sensor data information distribution. Probability of matching point position, detected between two images, (a) and (b), corresponding to two poses of the robot.

3.3 System Operation

The overall system operation, comprising all the presented contributions is depicted in Fig. 6, where the work flow is: (*i*) image acquisition; (*ii*) multi-scaled distribution (scaling factor); (*iii*) predicted movement and uncertainty propagation; (*iv*) Bayesian inference to weight the final matched points.

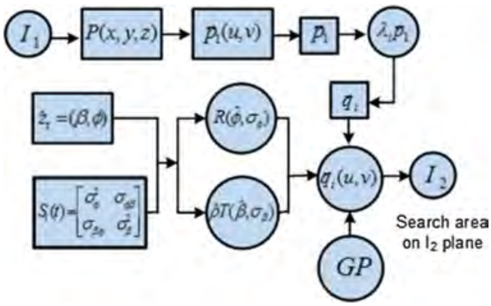

Fig. 6. System operation sustained by the proposed contributions.

4 Omnidirectional Localization on vSLAM

This section briefly introduces the final application where the omnidirectional localization is embedded. It consists of a view-based SLAM approach, which it is synthesized in Fig. 7. The key aspect lays on a dual 2D-3D map composed by a reduced set of omnidirectional views acquired at different poses, $x_n = (\mathrm{x}, \mathrm{y}, \theta)_n^T$, along the path of the robot. Each n view compresses the visual information of an area of the environment by means of a set of SURF feature points [1]. The

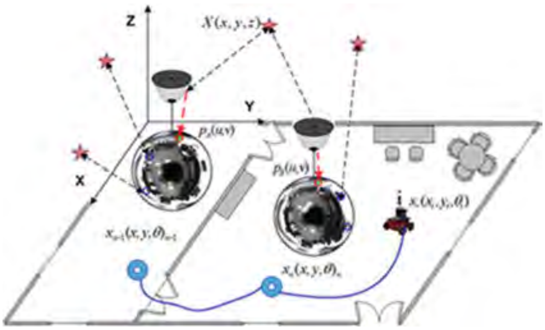

Fig. 7. Dual 2D-3D. Information is encoded on the 2D image plane by feature points on each view, x_n. The re-estimation of x_n implies the whole re-estimation of the map.

current pose of the robot at t is expressed as $x_r = (\mathrm{x}_t, \mathrm{y}_t, \theta_t)^T$. Therefore, the state vector comprises x_r and x_n, with the following 2D structure:

$$x_v(t) = \left[x_r \; x_1 \cdots x_n \cdots x_N\right]^T \tag{12}$$

with each view $n \in [1, \ldots, N]$. Then the state vector encodes a map constituted by a total number of N views.

The information is compressed on the 2D image frame by feature points. However, they express the same information that 3D landmark-based approaches [5, 8]. Now it is not necessary to re-estimate the 3D pose of every landmark in the environment. Here, the single re-estimation of a view, as part of $x_v(t)$, already implies the whole re-estimation of the map, being now much simpler. It is worth noticing that each x_n accounts for the visual encoding of a specific area of the environment, so that the robot can always localize itself. Finally, this vSLAM approach is subdivided into three main stages: (*i*) initialization of views in the map; (*ii*) observation model measurement; (*iii*) data association. Dealing with localization makes us only focus on (*ii*), since it provides the localization of the robot within the current estimated map.

4.1 Observation Model

Similarly to Sect. 2, the observation measurements expresses the motion transformation between two images (β,ϕ), and so does between two poses of the robot. Transferring this localization relation into the robot reference system, leads to the following structure, where is worth noting the $z_{t,n}$ corresponds to the application of the presented contributions for omnidirectional localization in Sect. 3.

$$z_{t,n} = \begin{pmatrix} \phi \\ \beta \end{pmatrix} = \begin{pmatrix} \arctan\left(\frac{\mathrm{y}_n - \mathrm{y}_t}{\mathrm{x}_n - \mathrm{x}_t}\right) - \theta_t \\ \theta_n - \theta_t \end{pmatrix} \tag{13}$$

5 Results

This section provides a further insight into the contributions presented in this work. Here, real data experiments have been conducted in order to show the benefits of this proposal for omnidirectional localization. Besides, the performance of a vSLAM has been also analyzed, when the omnidirectional localization is embedded. The equipment was presented in Sect. 2 and Fig. 1 ($2 \times$ 1.7 Ghz/2 Gb RAM). The real dataset comprises indoor office and laboratory-like spaces [16] (1238 images/123.8m path).

5.1 Omndirectional Localization Results

Firstly, we present results solely based on the proposed omnidirectional localization aiming at validation. Figure 8 presents performance results comparing a standard omnidirectional localization and the proposed in this work (average

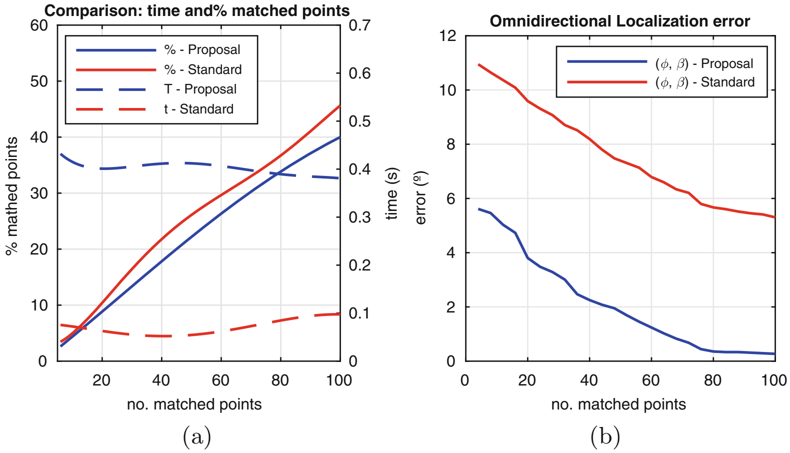

Fig. 8. Omnidirectional localization results. (a) % matched points and time consumption with total number of matched points. (b) Localization error.

values over 100 times execution). Figure 8(a) compares the % matched points out of the total feature points in two images (Y-left-axis), time consumed (Y-right-axis), and the total number of matched points (X-axis). Note the reduction (∼9%) with the proposed approach, which corresponds to a great false positive reduction, since the delimited search area on the image. Obviously, this comes at a cost of computation. Nonetheless, the consumption proves to be stable and acceptable for real time, regardless the number of matchings. Secondly, Fig. 8(b) shows a comparison of accuracy, in terms of angular error. The presented approach proves to outperform standard omnidirectional localization (∼10% average). These measurements shows the average error on the estimated localization (β,ϕ), (13). Note that 10% of angular improvement implies higher accuracy on the XY-coordinates, due to the parallax effect. Therefore, subtle improvements on the angular localization may be enough to ensure convergence on a generic vSLAM application.

5.2 vSLAM Results

Then it is necessary to test the approach when operating in vSLAM. Consequently, we conducted a real experiment in a sub-environment within [16]. The observation measurement $z_{t,n}$ (13), now embeds the proposed omnidirectional localization. Figure 9 shows real data results obtained in a 20 × 20m scenario. Figure 9(a) demonstrates that the proposed vSLAM approach, outperforms a standard one in terms of accuracy. This is a reliable proof to confirm that subtle variations on the accuracy of the localization may cause the final estimation to diverge. Besides, Fig. 9(b) presents average error results (RMSE), when the number of matching is varied. These results confirm that a tradeoff setup with low number of matching points may produce a well-balanced and feasible estimation.

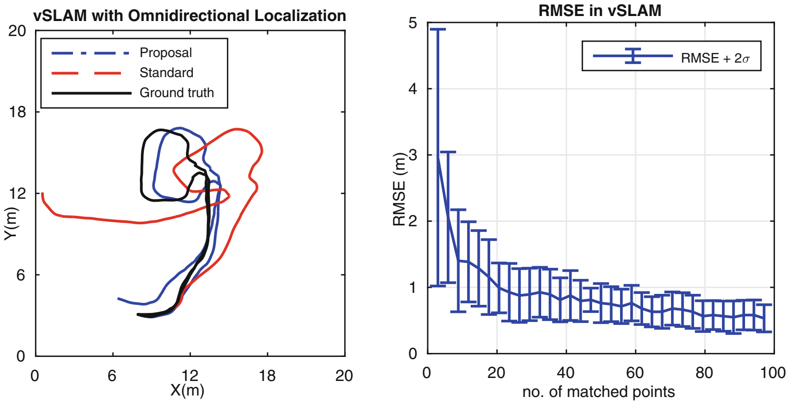

(a) (b)

Fig. 9. Real data vSLAM results. (a) Estimation with the proposed approach (blue), standard (red), and ground truth (dark). (b) RMSE (m) with the number of matchings. (Color figure online)

6 Conclusions

This article proposes a robust visual localization, based on omnidirectional images, for mobile robotics. The main contribution consists of an advantageous matching which dynamically adapts to the changing uncertainty circumstances in the system. Besides, GPs have been introduced to infer a sensor data distribution. In particular, we have produced a probability distribution for the location of matching points. Overall, we have devised a reliable approach which reduces considerably the search area for matching points. Moreover, an adaption of the epipolar constraint has been designed in order to fulfill the omnidirectional geometry. All contributions have been jointly implemented so as test the validity and feasibility of the omnidirectional localization over real data experiments, in vSLAM. A certain computation effort is needed, however the benefits reveal a valuable false positive avoidance ($\sim$9%) and a reinforcement of the localization accuracy ($\sim$10%). These values are referred to angular localization, fact that makes XY-localization more precise, due to the parallax effect. In vSLAM, such % of improvement implies a great step forward in order to ensure convergence on the estimation at each t.

References

1. Bay, H., Tuytelaars, T., Van Gool, L.: Speeded up robust features. Comput. Vis. Image Underst. **110**, 346–359 (2008)
2. Brand, C., Schuster, M.J., Hirschmller, H., Suppa, M.: Submap matching for stereo-vision based indoor/outdoor slam. In: IEEE IROS, pp. 5670–5677 (2015)
3. Brown, M.Z., Burschka, D., Hager, G.D.: Advances in computational stereo. IEEE Trans. PAMI **25**(8), 993–1008 (2003)

4. Caruso, D., Engel, J., Cremers, D.: Large-scale direct slam for omni directional cameras. In: IEEE IROS, pp. 141–148 (2015)
5. Davison, A.J.: Real-time simultaneous localisation and mapping with a single camera. In: ICCV, vol. 2, pp. 1403–1410, France (2003)
6. Engel, J., Stuckler, J., Cremers, D.: Large-scale direct slam with stereo cameras. In: IEEE IROS, pp. 1935–1942 (2015)
7. Ghaffari Jadidi, M., Valls Miro, J., Valencia, R., Andrade-Cetto, J.: Exploration on continuous Gaussian process frontier maps. In: IEEE ICRA, pp. 6077–6082, China (2014)
8. Gil, A., Reinoso, O., Ballesta, M., Juliá, M., Payá, L.: Estimation of visual maps with a robot network equipped with vision sensors. Sensors **10**, 5209–5232 (2010)
9. Hartley, R., Zisserman, A.: Multiple View Geometry in Computer Vision. Cambridge University Press, Cambridge (2004)
10. Huang, S., Dissanayake, G.: Convergence and consistency analysis for extended Kalman filter based slam. IEEE Trans. Rob. **23**(5), 1036–1049 (2007)
11. Joly, C., Rives, P.: Bearing-only SAM using a minimal inverse depth parametrization. In: ICINCO, vol. 2, pp. 281–288 (2010)
12. Kulback, S., Leiber, R.A.: On information and sufficiency. Ann. Math. Stat. **22**, 79–86 (1951)
13. Lee, S.J., Song, J.B.: A new sonar salient feature structure for EKF-based slam. In: IEEE IROS, pp. 5966–5971 (2010)
14. Leung, C., Huang, S., Dissanayake, G.: Active slam in structured environments. In: IEEE ICRA, pp. 1898–1903 (2008)
15. Longuet-Higgins, H.C.: A computer algorithm for reconstructing a scene from two projections. Nature **293**(5828), 133–135 (1985)
16. Paya, L., Amoros, F., Fernandez, L., Reinoso, O.: Performance of global-appearance descriptors in map building and localization using omnidirectional vision. Sensors **14**, 3033–3064 (2014)
17. Rasmussen, C.E., Williams, C.K.I.: Gaussian processes for machine learning. In: Adaptive Computation and Machine Learning series. Massachusetts Institute of Technology (2006)
18. Scaramuzza, D., Martinelli, A., Siegwart, R.: A toolbox for easily calibrating omni directional cameras. In: IEEE IROS, pp. 5695–5701, China (2006)
19. Servos, J., Smart, M., Waslander, S.: Underwater stereo slam with refraction correction. In: IEEE IROS, pp. 3350–3355 (2013)
20. Shuang, Y., Baoyuan, C., Lei, Z., Xiaoyang, Y., Haibin, W., Jixun, Z., Deyun, C.: Encoded light image active feature matching approach in binocular stereo vision. In: IFOST, pp. 406–409 (2016)
21. Valiente, D., Gil, A., Fernandez, L., Reinoso, O.: A modified stochastic gradient descent algorithm for view-based slam using omnidirectional images. Inf. Sci. **279**, 326–337 (2014)